European Journal of Integrative Medicine 22 (2016) 539–547

Contents lists available at ScienceDirect

Nano Energy

journal homepage: www.elsevier.com/locate/nanoenergy

Full paper

High performance thin film solar cells on plastic substrates with nanostructure-enhanced flexibility

Qingfeng Lin [a], Linfeng Lu [b], Mohammad Mahdi Tavakoli [a], Chi Zhang [b], Ga Ching Lui [a], Zhuo Chen [a], Xiaoyuan Chen [b], Lei Tang [a], Daquan Zhang [a], Yuanjing Lin [a], Paichun Chang [c], Dongdong Li [b,*], Zhiyong Fan [a,*]

[a] Department of Electronic and Computer Engineering, The Hong Kong University of Science and Technology, Clear Water Bay, Kowloon, Hong Kong SAR, China
[b] Shanghai Advanced Research Institute, Chinese Academy of Sciences, 99 Haike Road, Zhangjiang Hi-Tech Park, Pudong, Shanghai 201210, China
[c] Department of Creative Industry, Kainan University, No. 1, Kainan Road, Luchu, 338 Taoyuan County, Taiwan, ROC

ARTICLE INFO

Article history:
Received 21 January 2016
Received in revised form
18 February 2016
Accepted 21 February 2016
Available online 2 March 2016

Keywords:
Thin film solar cells
Plastic substrates
Nanocone
High performance
Flexibility

ABSTRACT

Plastic substrates possess conspicuous advantages for flexible thin film solar cell applications due to their superior flexibility and light weight characteristics. However, there are several challenges of using plastic substrates for high performance thin film solar cells since they usually have low melting/softening temperature and high coefficient of thermal expansion (CTE). In this work, we demonstrated a low cost process to achieve regular nanocone arrays on polyimide (PI) substrates which have unique photon management property and excellent mechanical flexibility. To leverage these benefits of the nanocone substrates, flexible amorphous Si solar cells were fabricated on the structures. Intriguingly, it was discovered that properly designed nanocones can significantly improve solar cell device performance via light management. And the fabrication yield of properly designed nanocone solar cells is much higher than that of planar devices. In addition, the nanocone plastic solar cells possess much improved bendability and robustness verified by both experiment and mechanical modeling, showing unique stress release mechanism originated from three-dimensional nanostructure design. This property is of practical significance for flexible electronics not limited to solar cells.

1. Introduction

Photovoltaic (PV) devices, which directly convert solar energy into electricity, have gained considerable interest worldwide as promising candidates for harvesting clean and renewable solar energy. Global cumulative photovoltaic capacity has grown exponentially for more than two decades, sufficient to supply 1 percent of global electricity demands by the end of 2014 [1]. Thin film solar cells are tremendously attractive for low cost applications, due to small material consumption and low temperature processes, as compared with the conventional crystalline Si-based PV devices. Particularly, light-weight and mechanically flexible thin film solar cells enable a wide range of potential applications from building-integrated PV generation to portable energy sources [2–4]. There are a number of choices of substrates for flexible thin film solar cells, such as metallic foils, thin glasses and plastics [2,5–13]. With the superior flexibility and light weight characteristics, plastic substrates possess conspicuous advantages for wearable and aerospace/space applications [4,10,12,14]. However, there are several challenges of using plastic substrates for high performance thin film solar cells. For example, they usually have low melting/softening temperature and high coefficient of thermal expansion (CTE). Low melting/softening temperature limits the processing temperature for high efficiency solar cells based on materials including Si, CdTe, CIGS and perovskite thus leading to moderate energy conversion efficiency of the devices [15–20]. Meanwhile, higher CTE of the supporting plastic substrate than the atop photovoltaic active layers may incur stress and strain accumulation in the thin films thus leading to device failure or fast performance degradation. In this work, we demonstrate a low cost and scalable approach to achieve regular nanocone arrays on polyimide (PI) substrates, on which thin film hydrogenated amorphous silicon (*a*-Si:H) solar cells were directly fabricated with decent device performance. It is worth pointing out that among all plastic materials, PI has high thermal stability and excellent mechanical flexibility thus is promising as a substrate material for flexible electronic devices [9,15,17,21,22]. In our process, liquid PI solution was used to cast nanocone-structured films without relying on

* Corresponding authors.
E-mail addresses: lidd@sari.ac.cn (D. Li), eezfan@ust.hk (Z. Fan).

http://dx.doi.org/10.1016/j.nanoen.2016.02.042
2211-2855/

complicated and costly lithographic techniques. Several unique advantages of utilizing PI nanocones for thin film solar cells have been discovered in this work. Intriguingly, it was found that properly designed nanocones can significantly improve solar cell device performance. Particularly, device power conversion efficiency (PCE) was found almost doubled on the optimized nanocone structures, as compared with the device fabricated on a flat substrate prepared with the same solution process. Even compared with the devices fabricated on commercial flat PI substrates, the nanocone devices still outperform by 48%. Meanwhile, it was discovered that the fabrication yield of properly designed nanocone solar cells is much higher than the flat devices. The large improvement on device performance and fabrication yield can be rationalized by a combinational effect of superior light trapping capability and the thermal strain/stress release. Moreover, it was found that the nanocone plastic solar cells possess much improved flexibility and robustness as opposed to the flat devices. Experiment and mechanical modeling showed that the nanotexturized substrate helps to significantly reduce the stress and strain inside a solar cell device induced by mechanical bending. Note that this phenomenon has not been reported before and it is of practical importance for flexible electronics not limited to solar cells. Overall, this work demonstrates a viable and convenient route toward low cost fabrication of efficient and robust flexible thin film solar cells. Although *a*-Si:H is used as the model material in this work, the developed nanocone plastic substrates can also be used for other types of thin film PV devices, such as organic solar cells as well as emerging high performance perovskite solar cells.

2. Materials and methods

2.1. Materials

Aluminum foil (0.25 mm thick, 99.99% purity) was purchased from Alfa Aesar, liquid polyimide solution (PI-2525) was purchased from HD MicroSystems, commercial flat polyimide film (Kapton® B, 25.4 μm thick) was provided by DuPont. All other chemicals are products of Sigma-Aldrich.

2.2. Flexible nanocone PI substrates assembly

An electrochemically polished clean Al foil was mechanically imprinted using a silicon stamp with hexagonally ordered nanopillars with height of 200 nm and tunable pitch of 500 nm–2 μm to produce a nanoindentation array on the surface of the Al foil. Thereafter, the i-cone array was fabricated by a multi-step anodization and wet etching process on the imprinted Al foil in an acidic solution with a proper direct-current (DC) voltage [23–25]. Afterwards, a 100 nm thick SiO_2 film was deposited on the as-obtained i-cone AAO template by PECVD at 150 °C as an anti-sticking layer between the i-cones AAO and PI for easy peeling off of PI film from the template subsequently. Thereafter, liquid PI solution (PI-2525) was spin coated onto the SiO_2-coated template at 50 rpm for 1.5 mins, followed by three baking steps (30 mins for each step) with temperatures of 100 °C, 150 °C and 170 °C on a hot plate to solidify the PI solution in air. After the sample cooled down to room temperature, the solidified PI film was carefully peeled off from the AAO template and then sandwiched in between silicon wafers and placed in an oven for higher temperature curing. The curing temperature gradually rose up to 200 °C with a ramping rate of 4 °C/min, then maintained at 200 °C for 30 mins, followed by increasing the temperature to 350 °C with a ramping rate of 2.5 °C/min. Then the PI film was curing at 350 °C for 4 hrs before natural cooling. An argon flow was maintained at 400 sccm during the curing process in the oven. Finally, the fully cured PI substrates were immersed in buffered oxide etch (BOE) solution for 10 mins to remove potential SiO_2 residue on the surface.

2.3. Fabrication of a-Si:H solar cells

A Ag reflector layer was firstly deposited on a PI substrate by direct current (DC) magnetron sputtering at room temperature in argon plasma atmosphere. Then an AZO spacer layer was sputtered by radio frequency (RF) magnetron sputtering of a 2 wt% Al_2O_3 doped ZnO ceramic target (99.99% purity) under argon plasma at a base temperature of 150 °C. Subsequently, a stack of *n*-*i*-*p* *a*-Si:H layers were successively deposited in a multi-chamber PECVD system consisting of three PECVD chambers. All these chambers have identical capacitively coupled parallel-plate electrode configurations and serve for the deposition of intrinsic, *n* doped and *p* doped layer, respectively. The *a*-Si:H absorber layers were prepared from a mixture of SiH_4 and H_2 gases at an excitation frequency of 40 MHz. Doping was achieved by gas mixture of hydrogen-diluted phosphine (PH_3) for deposition of *n* layer and hydrogen-diluted diborane (B_2H_6) for *p* layer at an excitation frequency of 13.56 MHz. After device fabrication, an 80 nm thick ITO layer was deposited by RF sputtering as top electrode.

2.4. Device characterization

SEM images of the thin film *a*-Si:H PV devices were obtained by a JEOL JSM-6700F SEM working at 5 kV. Angular and wavelength dependent absorption spectra of all devices were performed with a home-built Ultra-violet/Visible measurement system. All the *J*–*V* curves of thin film *a*-Si:H solar cells were carried out using a solar simulator (Newport corporation, 91150V) under 1 sun illumination. The EQE measurements were characterized by Oriel QE-PV-SI (Newport Corporation).

3. Results and discussion

The fabrication procedure of thin film *a*-Si:H solar cells on nanocone PI substrates is schematically illustrated in Fig. 1a1–a4. Firstly, a highly ordered anodic aluminum oxide (AAO) template with an inverted nanocone (i-cone) array was fabricated (Fig. 1a1) *via* a multi-step anodization and wet etching process on the imprinted Al foil [23–25]. Note that the pitch and aspect ratio of the i-cones fabricated with this approach are largely tunable, as we have reported recently [24–30]. A 100 nm thick SiO_2 layer was then deposited on the as-obtained i-cone AAO template by plasma enhanced chemical vapor deposition (PECVD) at 150 °C as an anti-adhesion layer followed by spin coating of PI solution on the surface, as shown in Fig. 1a2. Then the PI solution coated AAO template was partially cured on a hot plate to solidify the PI solution in air with gradual increased curing temperature up to 170 °C. Thereafter, the solidified nanocone PI film (Fig. 1a3) was carefully peeled off from the i-cone AAO template. Afterward, the nanocone PI film (~100 μm thick) was further cured in an oven up to 350 °C for 4 hrs. Finally, a thin film *a*-Si:H *p*–*i*–*n* junction solar cell was fabricated on the fully cured nanocone PI substrate, as shown in Fig. 1a4. The detailed fabrication process can be found in the Experimental Section and Fig. 1a4 indicates each layer in the device. Note that, a Ag layer was used at the bottom of device as a back reflector and also bottom electrode. An 80 nm thick aluminum doped zinc oxide (AZO) layer serves as a buffer layer to reduce the metal diffusion into the silicon layer [31–33]. Fig. 1b–d shows scanning electron microscopy (SEM) images of the as-obtained thin film *a*-Si:H devices based on flat PI substrates prepared with the same solution process on a Si substrate (cross-sectional view), 1.2 μm pitch nanocone PI substrates with aspect ratios of

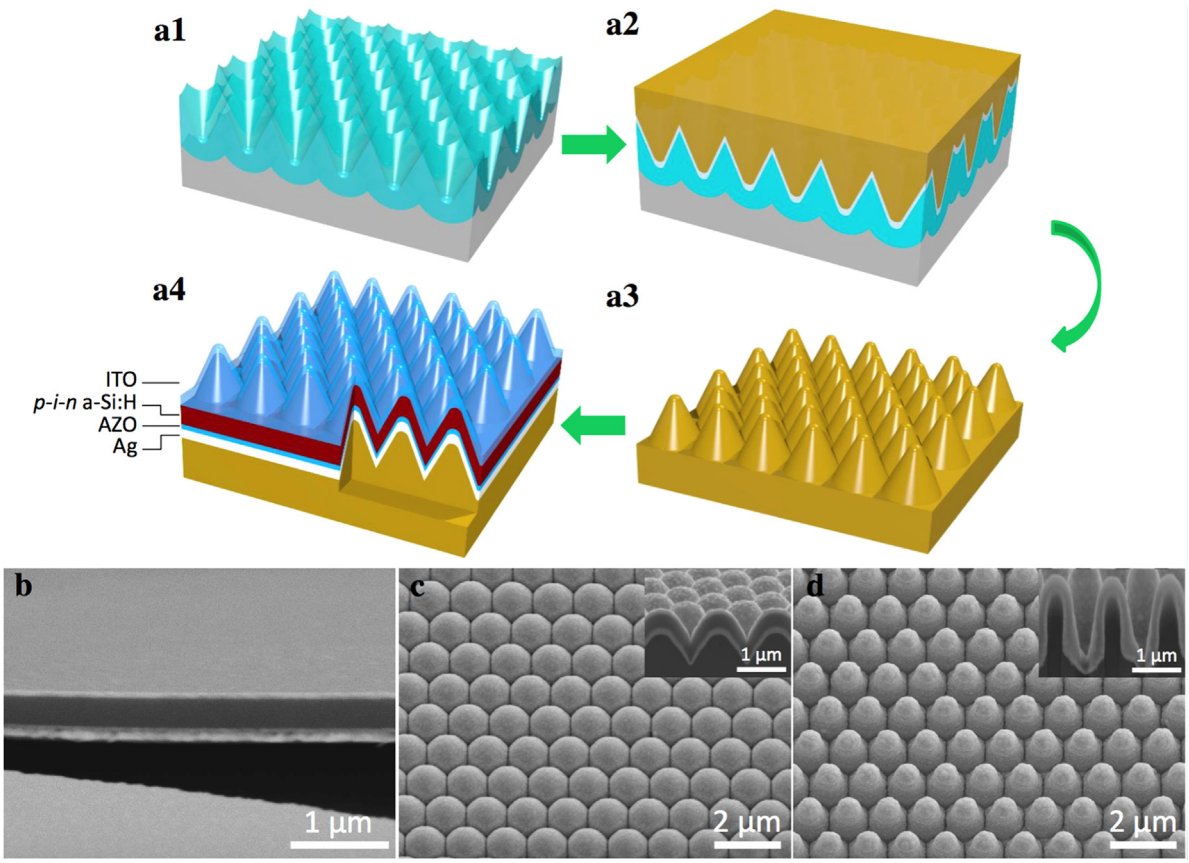

Fig. 1. Schematic fabrication procedure and SEM images of thin film *a*-Si:H soalr cells on nanocone PI substrates. (a1) The i-cone AAO template fabricated *via* a multi-step anodization and wet etching process on the imprinted Al foil. (a2) The spin coated PI solution on a SiO_2-coated i-cone AAO template. (a3) A solidified nanocone PI substrate peeled off from the i-cone AAO template. (a4) A thin film *a*-Si:H *p–i–n* junction solar cell fabricated on the fully cured nanocone PI substrate. SEM image of thin film *a*-Si:H soalr cells on (b) spin coated flat PI substrates (cross-sectional view), (c) 0.5 aspect ratio nanocone PI substrates (30° tilted-angle view, and cross-sectional view in the inset), and (d) 1.0 aspect ratio nanocone PI substrates (30° tilted-angle view, and cross-sectional view in the inset).

0.5 and 1.0 (30° tilted-angle view, and cross-sectional view in the insets), respectively. Note that the aspect ratio is defined as the ratio between the height and pitch of the nanocone arrays. The SEM images demonstrate that the *a*-Si:H devices based on flat and 0.5 aspect ratio nanocone PI substrates maintain excellent film conformality and uniformity, however the one based on 1.0 aspect ratio nanocone PI substrate results in poorer film uniformity.

Our previous research has shown that utilization of various three-dimensional nanostructures can substantially improve light capturing capability and PCE of solar cell devices [24–26,30,32,34]. To quantitatively investigate the light trapping effect of the nanocone structures, UV–vis reflectance spectra of the above three kinds of *a*-Si:H devices were measured with an integrating sphere [30]. The absorption spectra were achieved by subtracting reflectance from unity as the devices are opaque. Fig. 2a presents the normal incident absorption spectra of the three *a*-Si:H devices shown in Fig. 1b–d. It is known that a-Si has an optical band gap of ~1.7 eV, corresponding to ~720 nm optical wavelength. Therefore, spectral range 400–720 nm was chosen to investigate above-band-gap optical absorption of these devices. On the other hand, this wavelength range has covered the peak of solar irradiance, thus the results are meaningful for studying the optical properties of the PV devices. As clearly shown in Fig. 2a, the nanocone devices demonstrated much higher absorption capability than the flat one, meanwhile, the 0.5 and 1.0 aspect ratio devices showed quite close absorption efficiency over all wavelengths. In addition, the integrated absorption of these three devices is presented in Supporting Information Fig. S1a, which is obtained by integrating the absorption spectrum (Fig. 2a) with the AM1.5G photon flux spectrum [35] (Supporting Information Fig. S1b) in the wavelength range of 400–720 nm [29]. In order to further verify the experimental results, finite-difference-time-domain (FDTD) simulations were performed on these devices, resulting in the simulated absorption spectra of them as shown in Fig. 2b. The simulated absorption spectra show quite consistent trend over the entire wavelength range with the experimental ones among these three devices as described above. Moreover, to shed light on how light is coupled into these devices, the cross-sectional electric field intensity ($|E|^2$) distribution of the electromagnetic (EM) wave at 500 nm wavelength was plotted as shown in Fig. 2**c**. In these three simulation models, EM plane waves propagate downward from $Y=2$ μm and reach the top surfaces of these devices at $Y=1$ μm. Note that the color index at the specific location in the cross-sectional $|E|^2$ distribution indicates the magnitude of $|E|^2$ at that point, normalized with that of the source EM wave if propagating in free space. The different refractive index of the materials at 500 nm wavelength in the simulation devices are more clearly illustrated in Supporting Information Fig. S2. In order to observe the light propagation in each layer in the devices more easily, white dashed lines were plotted in Fig. 2c1–c3 to show the interfaces between each materials in the devices, and the materials were labelled on Supporting Information Fig. S2a. The fringe patterns in Fig. 2c below $Y=2$ μm originate from the interference between the source light and the reflected light. And the color index above $Y=2$ μm indicates the intensity of the reflected light. The cross-sectional $|E|^2$ distributions demonstrate lower reflection for the 0.5 and 1.0 aspect ratio nanocone devices (Fig. 2c1 and c2) than the flat device (Fig. 2c3), indicated by the darker color above light

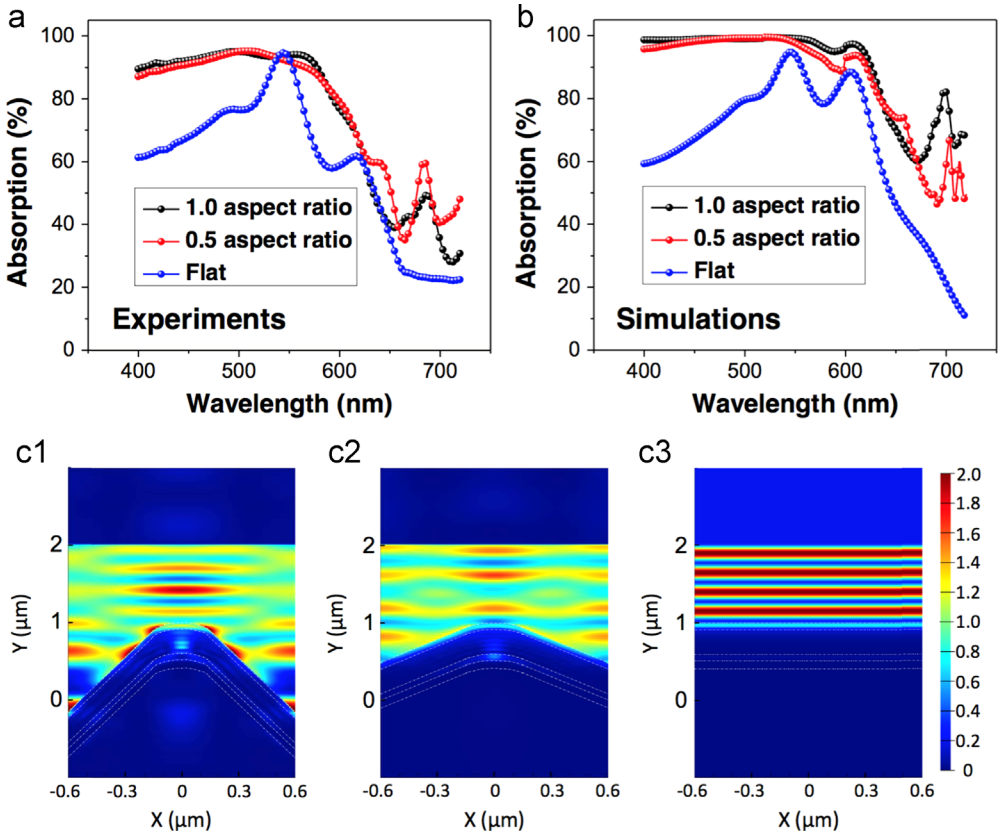

Fig. 2. (a) Experimental and (b) simulated absorption spectra of *a*-Si:H devices based on 1.2 μm pitch nanocone PI substrates with different aspect ratios and the flat reference. Simulated cross-sectional $|E|^2$ distribution of the EM wave at 500 nm wavelength in *a*-Si:H devices based on (c1) 1.0 aspect ratio nanocone PI substrates, (c2) 0.5 aspect ratio nanocone PI substrates, and c3) flat PI substrates.

source, which is consistent with the results in Fig. 2a and b. In addition, the absorption profiles of these devices in the active layers at 500 nm wavelength are illustrated in Supporting Information Fig. S3, demonstrating that most of the light absorption happens in the *a*-Si:H layer, which is beneficial for electron-hole pairs generation and collection.

The above optical investigation shows the potency of nanocones for efficient light absorption. Furthermore, the device performance of the three types of *a*-Si:H solar cells discussed above were characterized. In addition, the performance of thin film *a*-Si:H solar cells fabricated on commercial flat PI substrates were also studied as the reference. And the photograph of these four types of devices is demonstrated in Supporting Information Fig. S4. Fig. 3a demonstrates representative current density–voltage (*J*–*V*) characteristics of the four kinds of devices measured with a solar simulator (Newport Corporation, 91150V) under 1 sun illumination. Short-circuit current density (J_{sc}) and open circuit voltage (V_{oc}) extracted from these *J*–*V* curves are summarized in Table 1. The *J*–*V* curves demonstrate that the J_{sc} increases significantly from 9.13 mA/cm^2 to 12.95 mA/cm^2 as the aspect ratio increases from 0 (the flat device) to 0.5, primarily owing to the improved light absorption capability as shown in Fig. 2, while it declines to 11.59 mA/cm^2 when the aspect ratio further increases to 1.0. The trend for J_{sc} can also be confirmed with external quantum efficiency (EQE) measurements shown in Fig. 3b. Overall, the 0.5 aspect ratio nanocone device show the highest J_{sc}, fill factor and a decent V_{oc}, thus has the highest PCE of 7.06% as shown in Table 1, which is 94% higher than that of the flat device fabricated by spin coating. Even compared with the flat device fabricated on the commercial PI substrate with a PCE of 4.76%, the relative improvement of 48% is also substantial. It's worth pointing out that the 0.5 aspect ratio nanocone device has 30% higher integrated light absorption than the commercial flat device, leading to ~30% higher J_{sc}. In addition, it also has higher fill factor than the commercial flat device, resulting in overall ~50% improvement on the device efficiency. And the higher fill factor can be explained by mechanically more robust ITO electrodes with less crack lines than the flat device which will be discussed below. Intriguingly, it was also found that the properly designed nanocone structure can not only largely enhance device PCE, but also improve the device fabrication yield remarkably. Note that the device yield is defined as the percentage of devices with PCE larger than 1% in this work. As illustrated in Fig. 3c, the 0.5 aspect ratio nanocone devices have yield of 75%, which is three times of that for the flat devices fabricated on spin-coated PI substrates (25% yield). Meanwhile, the device yield on the commercial flat substrate and 1.0 aspect ratio nanocones are 50% and 17%, respectively, which are also much lower than the 0.5 aspect ratio nanocones devices. The device failure mechanism has been investigated. As shown in Fig. 3d and e, macroscopic crack lines can be easily identified from the as-fabricated flat *a*-Si:H solar cells on flat PI substrates while the devices on the 0.5 aspect ratio nanocone substrate are mostly crackline free. This is can be explained by the fact that the PI substrate has much higher coefficient of thermal expansion (CTE) as compared with the atop layers of Ag, AZO, *a*-Si:H and indium-doped tin oxide (ITO) (Supporting Information Table S1). As the highest temperature in the device fabrication process is 250 °C, the substrate heating and cooling steps introduce thermal strain and stress in each layers leading to formation of crack lines on the thin film eventually. However, on one hand, a nanocone substrate has much larger surface area than a flat substrate which improves overall adhesion between atop films and the substrate. On the other hand, as shown in Fig. 1c and d, solar cell thin films are effectively folded on the nanocone structure, thus the strain and

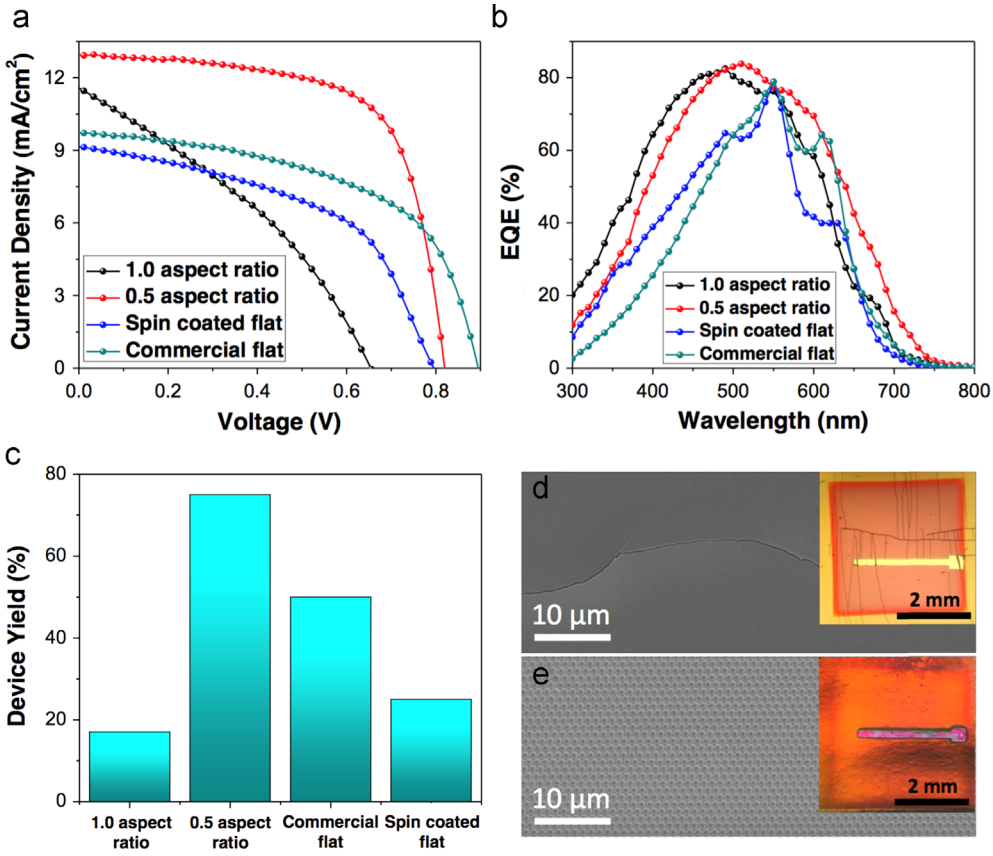

Fig. 3. (a) *J–V* curves and (b) EQE measurements of *a*-Si:H devices based on nanocone PI substrates with different aspect ratios and the flat reference cells. (c) Device yield of *a*-Si:H solar cells based on different PI substrates. SEM images and optical photographs (inset) of *a*-Si:H devices based on (d) spin coated flat PI substrates, and (e) 0.5 aspect ratio nanocone PI substrates.

Table 1
Summary of device performance of thin film *a*-Si:H solar cells based on different PI substrates.

Device	V_{oc} (V)	J_{sc} (mA/cm^2)	Fill Factor (%)	Efficiency (%)
Spin coated flat	0.797	9.13	50.1	3.64
Commercial flat	0.895	9.72	54.7	4.76
0.5 aspect ratio	0.820	12.95	66.5	7.06
1.0 aspect ratio	0.652	11.59	34.7	2.62

stress can be released when the underlying substrate expands or shrinks. This hypothesis will be further examined in the later part of this article supported by mechanical modeling results.

In addition to the above findings, we have also noticed that 1.0 aspect ratio nanocone devices have the lowest PCE and yield. This is due to the poor uniformity of a-Si layer coating on high aspect ratio structure and it is consistent with our previous reports [24,36,37]. Also, it was found that the device PCE and yield of the solar cells based on the spin coated flat PI substrates is lower than that on the commercial flat PI substrate. To shed light on this phenomenon, thermogravimetric analysis (TGA) of these two kinds of flat PI substrates was carried out, with the result shown in Supporting Information Fig. S5. The TGA results demonstrated that the spin coated flat PI substrates had slightly larger weight loss during the device fabrication processes (up to 250 °C) possibly due to residual solvent release. This may lead to poorer device performance and yield.

The above optical property investigations and device performance characterizations were performed with normal light incidence, while for practical operation, the angle of solar irradiation changes over the time in a day. Therefore, optical properties and device performances for angular incidence should be examined. In this regard, we characterized the angular dependent integrated light absorption and energy conversion efficiency of the device on 0.5 aspect ratio nanocone PI substrate, together with the one on our home-made flat PI substrate fabricated with spin coating for the sake of comparison. Fig. 4a presents the integrated absorption of the nanocone device and flat device for the light incident angles tuning from 0° (normal incident) to 60° with 10° interval using an integrating sphere and a broadband halogen light source. It can be clearly seen that the nanocone device possesses a much higher integrated absorption than the flat device over all incident angles, with an absolute enhancement of ~15% with small dependence on incident angle. Furthermore, energy conversion efficiency of these two devices at different incident angles were also measured and plotted in Fig. 4b, where the nanocone device demonstrates a substantial improvement of energy conversion efficiency over all incident angles compared to the flat counterpart. Overall, the nanocone device can enhance the light absorption and energy conversion efficiency omnidirectionally, because of the wavelength and angular independent anti-reflection effect of the nanocones due to the gradual change of effective refractive index of the entire nanostructures. The omnidirectional improvement of light absorption and energy conversion efficiency is of significance for practical deployment of solar panels without a costly solar tracking system.

Thus far, we have demonstrated that properly engineered nanocones improved the device performance and fabrication yield. As our devices have been fabricated on plastic substrates, characterization of flexibility/bendability is of paramount importance. Interestingly, it was found that nanocone structure could largely

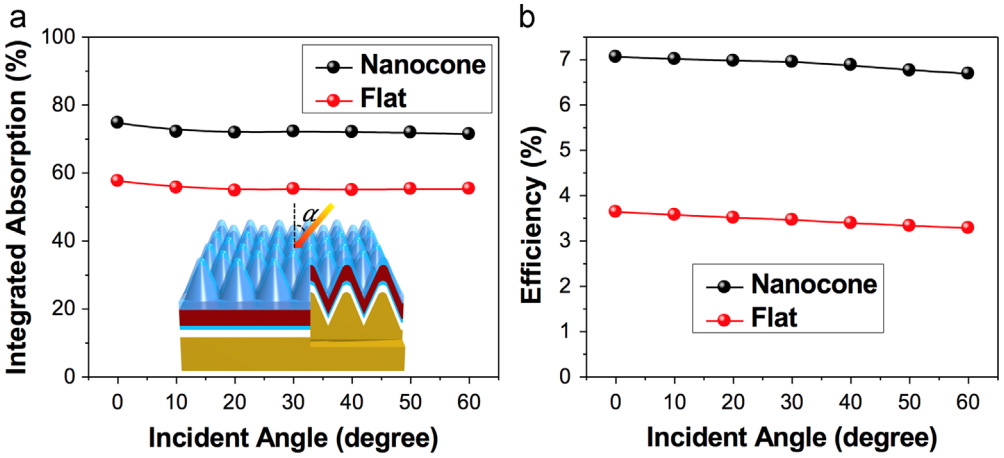

Fig. 4. (a) Integrated absorption and (b) energy conversion efficiency of the device on the 0.5 aspect ratio nanocone PI substrate and the spin coated flat PI substrate.

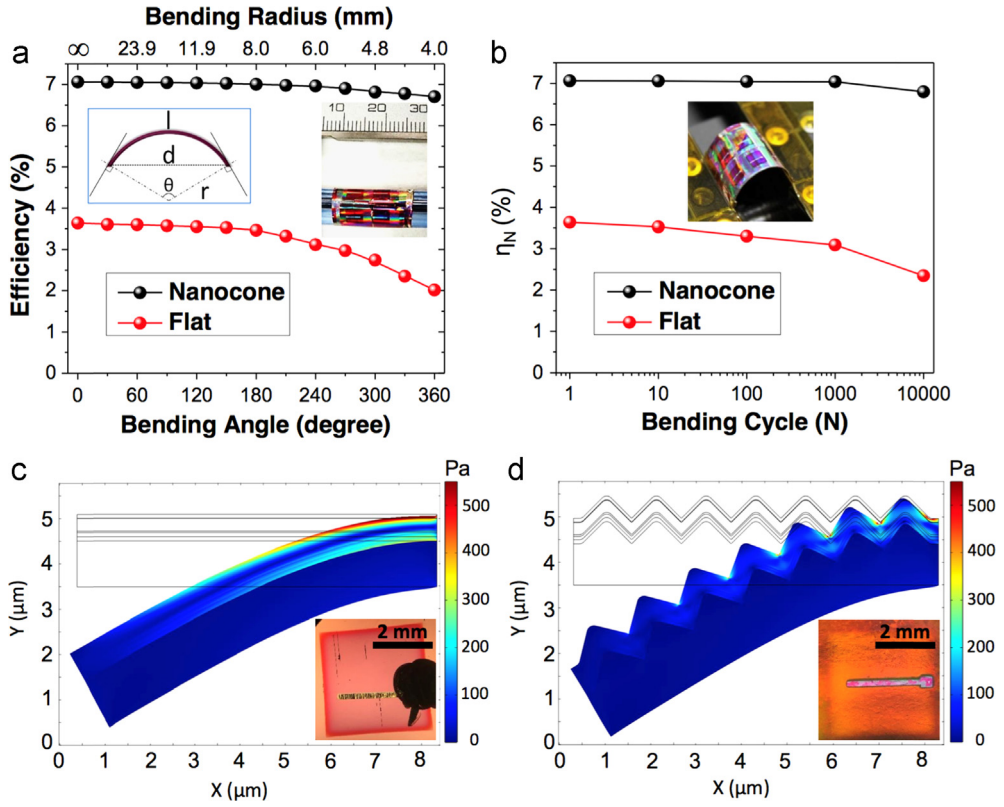

Fig. 5. Energy conversion efficiency of the PV devices based on 0.5 aspect ratio nanocone PI substrate and flat PI substrate (a) under different bending angles/radii and (b) after different bending cycles. Simulated cross-sectional stress distribution of (c) flat and (d) nanocone devices under bending, with their optical photographs after being bended with a curvature radius of 4 mm shown in the insets.

enhance flexibility and bendability of thin film PV devices on plastic PI substrates in this work. To demonstrate the robustness of the PV devices on nanocone plastic substrates, the PCE of the device on 0.5 aspect ratio nanocone PI substrate and the one on flat PI substrate under a bending angle θ from 0° to 360° (definition of θ is shown in the inset of Fig. 5a) was plotted in Fig. 5a. Evidently, the nanocone PV device efficiency demonstrates a negligible drop even at large bending angle, which is much better than its flat counterpart. The bending radius was also labeled on the upper X axis for better reference according to the equation $r=\frac{l}{\theta}$. Note that the PV devices characterized here have a length of 25 mm. So the nanocone device was bended with a curvature radius up to 4 mm when the bending angle is 360°, as shown in the inset photograph of Fig. 5a, while maintaining ~95% of the initial efficiency. This result shows the excellent bendability of the flexible device. Note that the light illumination area of the device was decreased when the bending radius was reduced. This led to reduction of the input optical power on the device. Therefore, the device energy conversion efficiency was calibrated by considering the change of the device actual projection area. Besides, the reliability of nanocone solar cells under multiple bending cycles was examined with an automatic bending setup as recorded in Supporting information Video S1, with the results presented in Fig. 5b. Each bending cycle was performed under 180° as shown in the inset of Fig. 5b, while the nanocone device still retained ~96% of the initial efficiency after 10,000 bending cycles however the flat device performance dropped to 64% after 10,000 bending cycles.

Supplementary material related to this article can be found online at http://dx.doi.org/10.1016/j.nanoen.2016.02.042.

The device performance degradation after different bending angles or multiple bending cycles as presented above results from the generated strain and stress in the thin films during bending, which increase the possibility of crack nucleation and delamination at the interface of the layers. To rationalize the much improved bendability and robustness of the nanocone solar cells, finite element modeling (COMSOL Multiphysics 4.2a finite element code) was carried out to investigate stress distribution in the device upon bending. The devices were modeled by Autodesk AutoCAD 2014 according to the SEM images (Fig. 1b and c) with dimensions of $8 \times 1.5\ \mu m^2$ as shown in Supporting Information Fig. S6a and b. Note that the thickness of the plastic substrate is set as 1 μm in order to reduce the simulation time. The right side of the device was anchored and $-3\ N/m^2$ load was applied to the other side as illustrated in Supporting Information Fig. S6c. Fig. 5c and d show the cross-sectional stress distribution for the flat and nanocone devices, respectively. The simulation results demonstrate that the stress concentration occurs between the layers of devices. In this regards, the textured device reveals much more uniform distribution of stress through all layers of the device as compared to the flat one especially in the interfacial regions, leading to lower possibility of crack nucleation in the films during bending. The ITO layer at the top and near to the anchored edge shows the highest stress due to its higher Young's modulus than the silicon layer underneath (more details can be found in Supporting information). The silicon and silver layers also indicate high tensile stress since they also have high Young's modulus but slightly lower than that of the ITO layer. Interestingly, the textured device illustrates lower stress through all layers compared with the flat one as shown in Fig. 5c and d, due to higher surface area in the interfacial regions between the layers. For instance, the maximum stress of ITO layer in the textured device occurs on the very small area; however the highest stress is distributed in a large area in the flat device. As a result, not only the level of stress but also the percentage of high stress regions distributed in the textured device is less than the flat one. In addition, it can be seen only a few areas with high stress concentration in textured device specially in the valleys regions, resulting in localized stress distribution and lower total strain energy. Thus this stress releasing mechanism can significantly improve the flexibility and durability of the textured device, especially when the device layers have different CTEs. To further support our results, the optical photographs of the flat and textured devices after being bended with a curvature radius of 4 mm are illustrated in the insets of Fig. 5c and d, and with their SEM images shown in Supporting Information Fig. S7. Evidently, a lot of crack lines exist on the surface of the flat device after being bended with a curvature radius of 4 mm, while they can be hardly found on the surface of the nanocone device. In a word, the nanocone structure can release the stress concentration through the layers, thus improve the flexibility and mechanical properties of the device. These results demonstrated the predominant flexibility and bendability of thin film solar cells on nanocone plastic substrates, which is essential for flexible PV applications, and other portable and personal electronic devices.

4. Conclusions

In summary, we have developed a low cost and scalable approach to fabricate regular nanocone arrays on PI substrate. The nanotextured substrate delivered higher thermal stability and excellent mechanical flexibility, thus is promising for flexible electronic devices. Thereafter, thin film *a*-Si:H solar cells were directly fabricated on the nanocone PI substrates to demonstrate their unique advantages on flexible thin film solar cells. Particularly, it was found that properly designed nanocone substrates can significantly improve solar cell device performance, with almost doubled PCE compared with the devices fabricated on flat substrates using the same solution process. Even compared with the devices fabricated on commercial flat PI substrates, the nanocone devices still outperform by 48%. Meanwhile, it was discovered that the fabrication yield of properly designed nanocone solar cells is much higher than flat devices. The large improvement on device performance and fabrication yield can be rationalized by a combinational effect of superior light trapping capability and the thermal strain/stress release. Moreover, it was found that the nanocone plastic solar cells possess much improved flexibility and robustness as opposed to the flat devices. Experiment and mechanical modeling showed that the nanotexturized substrate helps to significantly reduce the stress and strain inside a solar cell device induced by mechanical bending. This phenomenon has not been reported before and it is of practical importance for flexible electronics not limited to solar cells. Overall, this work demonstrates a viable and convenient route toward low cost fabrication of efficient and robust flexible thin film solar cells. Although *a*-Si:H is used as the model material in this work, the developed nanocone plastic substrates can also be extended to other types of thin film PV devices, and even other flexible electronics.

Acknowledgments

This work was supported by General Research Fund (612113) from Hong Kong Research Grant Council, Hong Kong Innovation and Technology Fund (ITS/117/13, ITS/362/14FP) from the Innovation and Technology Commission and State Key Laboratory on Advanced Displays and Optoelectronics at HKUST. We also acknowledge Science and Technology Commission of Shanghai Municipality, China (Grant no. 14JC1492900), the National Natural Science Foundation of China (Grant nos. 61474128 and 61504155), the Youth Innovation Promotion Association of the Chinese Academy of Sciences (2013302) and the Youth Innovation Fund for Interdisciplinary Research of SARI (Y426475234).

Appendix A. Supplementary material

Supplementary data associated with this article can be found in the online version at http://dx.doi.org/10.1016/j.nanoen.2016.02.042.

References

[1] M. Brunisholz, Snapshot of Global PV Markets 2014, The International Energy Agency Photovoltaic Power Systems Programme, Paris, 2015.
[2] Q. Lin, H. Huang, Y. Jing, H. Fu, P. Chang, D. Li, Y. Yao, Z. Fan, J. Mater. Chem. C 2 (2014) 1233–1247.
[3] Z. Fan, A. Javey, Nat. Mater. 7 (2008) 835–836.
[4] M.B. Schubert, J.H. Werner, Mater. Today 9 (2006) 42–50.
[5] J. Yang, A. Banerjee, S. Guha, Appl. Phys. Lett. 70 (1997) 2975–2977.
[6] X. Xu, T. Su, S. Ehlert, G. Pietka, D. Bobela, D. Beglau, J. Zhang, Y. Li, G. DeMaggio, C. Worrel, In: Proceedings of the 35th IEEE PVSC, 2010, pp. 001141–001146.
[7] Q.H. Fan, M. Deng, X. Liao, X. Deng, J. Appl. Phys. 105 (2009) 033304-033304-6.
[8] S. Hegedus, Prog. Photovolt. Res. Appl. 14 (2006) 393–411.
[9] A. Yusoff, M. Syahrul, K. Henkel, Bull. Mater. Sci. 30 (2007) 329–331.
[10] F. Liu K. Beernink C. Hu X. Xu A. Banerjee G. DeMaggio G. Pietka J. Yang S. Guha, In: Proceedings of the 33rd IEEE PVSC, 2008, pp.1–6.
[11] X. Xu, K. Lord, G. Pietka, F. Liu, K. Beernink, B. Yan, C. Worrel, G. DeMaggio, A. Banerjee, J. Yang, 33rd IEEE PVSC (2008) 1–6.
[12] A. Banerjee, X. Xu, K. Beernink, F. Liu, K. Lord, G. DeMaggio, B. Yan, T. Su, G. Pietka, C. Worrel, In: Proceedings of the 35th IEEE PVSC, 2010, pp. 002651–002655.

[13] M.M. Tavakoli, K. Tsui, S. Leung, Q. Zhang, J. He, Y. Yao, D. Li, Z. Fan, ACS Nano 9 (2015) 10287.
[14] M. Kaltenbrunner, G. Adam, E.D. Głowacki, M. Drack, R. Schwödiauer, L. Leonat, D.H. Apaydin, H. Groiss, M.C. Scharber, M.S. White, Nat. Mater. 14 (2015) 1032–1039.
[15] C. Yang, C. Hsueh, D. Yeh, C. Ho, C. Leu, Y. Yeh, S. Lee, IEEE Electron Device Lett. 32 (2011) 1254–1256.
[16] A. Tiwari, A. Romeo, D. Baetzner, H. Zogg, Prog. Photovolt. Res. Appl. 9 (2001) 211–215.
[17] A. Chirilă, S. Buecheler, F. Pianezzi, P. Bloesch, C. Gretener, A.R. Uhl, C. Fella, L. Kranz, J. Perrenoud, S. Seyrling, Nat. Mater. 10 (2011) 857–861.
[18] P. Docampo, J.M. Ball, M. Darwich, G.E. Eperon, H.J. Snaith, Nat. Commun. 4 (2013) 2761.
[19] D. Liu, T.L. Kelly, Nat. Photonics 8 (2014) 133–138.
[20] M.M. Tavakoli, Q. Lin, S. Leung, G.C. Lui, H. Lu, L. Li, B. Xiang, Z. Fan, Nanoscale 8 (2016) 4276–4283.
[21] K. Takei, T. Takahashi, J.C. Ho, H. Ko, A.G. Gillies, P.W. Leu, R.S. Fearing, A. Javey, Nat. Mater. 9 (2010) 821–826.
[22] C. Wang, D. Hwang, Z. Yu, K. Takei, J. Park, T. Chen, B. Ma, A. Javey, Nat. Mater. 12 (2013) 899–904.
[23] Q. Lin, S. Leung, K. Tsui, B. Hua, Z. Fan, Nanoscale Res. Lett. 8 (2013) 268.
[24] Q. Lin, S. Leung, L. Lu, X. Chen, Z. Chen, H. Tang, W. Su, D. Li, Z. Fan, ACS Nano 8 (2014) 6484–6490.
[25] S.F. Leung, M. Yu, Q. Lin, K. Kwon, K.L. Ching, L. Gu, K. Yu, Z. Fan, Nano Lett. 12 (2012) 3682–3689.
[26] K.H. Tsui, Q. Lin, H. Chou, Q. Zhang, H. Fu, P. Qi, Z. Fan, Adv. Mater. 26 (2014) 2805–2811.
[27] Y. Qiu, S. Leung, Q. Zhang, B. Hua, Q. Lin, Z. Wei, K. Tsui, Y. Zhang, S. Yang, Z. Fan, Nano Lett. 14 (2014) 2123–2139.
[28] J. Li, Y. Qiu, Z. Wei, Q. Lin, Q. Zhang, K. Yan, H. Chen, Z. Fan, S. Yang, Energy Environ. Sci. 7 (2014) 3651–3658.
[29] Q. Lin, B. Hua, S. Leung, X. Duan, Z. Fan, ACS Nano 7 (2013) 2725–2732.
[30] R. Yu, K. Ching, Q. Lin, S. Leung, D. Arcrossito, Z. Fan, ACS Nano 5 (2011) 9291–9298.
[31] C.M. Hsu, C. Battaglia, C. Pahud, Z. Ruan, F.J. Haug, S. Fan, C. Ballif, Y. Cui, Adv. Energy Mater. 2 (2012) 628–633.
[32] H. Huang, L. Lu, J. Wang, J. Yang, S. Leung, Y. Wang, D. Chen, X. Chen, G. Shen, D.D. Li, Z. Fan, Energy Environ. Sci. 6 (2013) 2965–2971.
[33] H. Xiao, J. Wang, H. Huang, L. Lu, Q. Lin, Z. Fan, X. Chen, C. Jeong, X. Zhu, D. Li, Nano Energy 11 (2015) 78–87.
[34] R. Kapadia, Z. Fan, K. Takei, A. Javey, Nano Energy 1 (2012) 132–144.
[35] National Renewable Energy Laboratory, Reference Solar Spectral Irradiance: Air Mass 1.5. http://rredc.nrel.gov/solar/spectra/am1.5/ (accessed 11, 2015) .
[36] S. Leung, L. Gu, Q. Zhang, K. Tsui, J. Shieh, C. Shen, T. Hsiao, C. Hsu, L. Lu, D. Li, Q. Lin, Z. Fan, Sci. Rep. 4 (2014) 4243.
[37] S. Leung, K. Tsui, Q. Lin, H. Huang, L. Lu, J. Shieh, C. Shen, C. Hsu, Q. Zhang, D. Li, Energy Environ. Sci. 7 (2014) 3611–3616.

Qingfeng Lin received his B.S. degree in electronic science and technology from University of Science and Technology of China in 2006. He received his Ph.D. degree in electronic and computer engineering from Hong Kong University of Science and Technology (HKUST) in 2014. Currently he works in HKUST as a postdoctoral research associate. His research interests include self-assembly of nanostructured functional materials and their applications for energy harvesting, energy storage, and nanoelectronics.

Linfeng Lu received his Ph.D. degree in Material Science from the Nanjing University of Aeronautics and Astronautics, in 2010. Currently, he works at Shanghai Advanced Research Institute, Chinese Academy of Sciences. His research interest focuses on semiconductor thin films for technological applications in photovoltaic devices.

Mohammad Mahdi Tavakoli is a Ph.D. student in the Department of Electronic and Computer Engineering at Hong Kong University of Science and Technology. He received his bachelor degree in Materials Science and Engineering from Iran University of Science and Technology in 2009. He obtained his master and Ph.D. degrees in Materials science and engineering from Sharif University of Technology in 2011 and 2015, respectively. His current research interest is about fabrication of perovskite thin film and nanowire for photovoltaic applications.

Chi Zhang is currently a joint Ph.D. candidate of Nanjing University of Science and Technology and Shanghai Advanced Research Institute, Chinese Academy of Sciences. His current research interest focuses on nanostructured optoelectronic thin film devices.

Ga Ching Lui is a research assistant in the Department of Electronic and Computer Engineering, Hong Kong University of Science and Technology. He receives his B.S. degree in Physics from the University of Science and Technology in 2014. His research interests include nanostructure fabrication and photovoltaics.

Zhuo Chen is an undergraduate student in the Department of Electronic and Computer Engineering, Hong Kong University of Science and Technology. He works in the Undergraduate Research Opportunities Program (UROP) under the project supervised by Prof. Zhiyong Fan. His current research interest is two-dimensional material electronics and nanophotonics.

Xiaoyuan Chen received a Ph.D. from the University of Strathclyde, UK in 1991 and has worked in both academia (Massachusetts Institute of Technology, University of Iowa, University of Cardiff) and industry (Corning) on semiconductor physics and devices. He joined the faculty at Shanghai Advanced Research Institute, Chinese Academy of Sciences in 2010. His research interests focus on photon, phonon and electron interactions in low-dimensional structures, and optoelectronic, and thermoelectric device application of these structures.

Lei Tang is a Mphil student in the Department of Electronic and Computer Engineering, Hong Kong University of Science and Technology. He received his B.S. degree in Material Processing and Control from University of Science and Technology Beijing, China, in 2014. His current research interests include nanostructure fabrication and anti-reflection films for photovoltaics.

Daquan Zhang is a Ph.D. student in the Department of Electronic and Computer Engineering, Hong Kong University of Science and Technology. He received his B.S. degree in Electronic Science and Technology from Wuhan University, Wuhan, China, in 2014. His current research interests include semiconductor NW array-based image sensor and perovskite photovoltaic devices.

Yuanjing Lin is a Ph.D. student in the Department of Electronic and Computer Engineering, Hong Kong University of Science and Technology. She received her B.S. degree in Electronic Science and Technology from Nankai University, Tianjin, China, in 2014. Her current research interests include nanostructure fabrication and energy storage system.

Paichun Chang received his M.S. degree of Electrical Engineering in 2004 and Ph.D. degree of Materials Science Engineering in 2008 from University of California, Irvine. He was a postdoctoral fellow in University of Southern California during 2009 and 2010, and worked on metallic nanowire sensor and nanowire based energy applications. He is an assistant professor in Kainan University, Taiwan. His research field includes surface treatments, 3D printing, and functionalized nanomaterials.

Dongdong Li received his Ph.D. degree in Materials Science from Shanghai Jiao Tong University in 2010. Under the support of Ministry of Education of the People Republic of China, he worked in the Department of Electrical Engineering at the University of Southern California (2007–2009). Currently, he is an associate professor at Shanghai Advanced Research Institute, Chinese Academy of Sciences. His research focuses on structural and interfacial engineering of functional nanomaterials, for technological applications in energy conversion and storage.

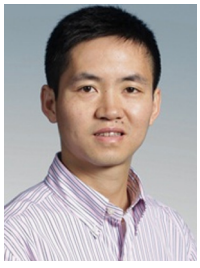

Zhiyong Fan received his B.S. and M.S. degrees in Physical Electronics from Fudan University, Shanghai, China, in 1998 and 2001. He received his Ph.D. degree from the University of California, Irvine, in 2006 in Materials Science. From 2007 to 2010 he worked in the University of California, Berkeley, as a postdoctoral fellow in the department of Electrical Engineering and Computer Sciences, with a joint appointment with Lawrence Berkeley National Laboratory. In May 2010, he joined Hong Kong University of Science and Technology as an assistant professor. His research interests include engineering novel nanostructures with functional materials, for technological applications including energy conversation, electronics and sensors, etc. (http://www.ece.ust.hk/~eezfan/index.htm).